Goddard Convective-Stratiform Heating (CSH) Algorithm

Wei-Kuo Tao, Steve Lang and Taka Iguchi

Latent heating (LH) cannot be measured directly with current techniques, including current remote sensing or *in situ* instruments, which explains why nearly all satellite retrieval schemes depend heavily on some type of cloud-resolving model or CRM (see review by Tao *et al.* 2006, 2016). This is true for the current CSH algorithm (Tao *et al*.. 1990, 1993, 2000, 2001, 2010; Lang and Tao, 2018; and Tao *et al*. 2019). Table 1 lists the highlights and references for the CSH algorithm over the course of its continued development.

Highlights	Reference
First paper to use a CRM to develop a LH algorithm - LH structure estimated from vertical hydrometeor profiles	Tao *et al.* (1990)
First paper on the CSH algorithm - composite both sounding estimated and CRM modeled convective and stratiform heating profiles into a simple look-up table (LUT)	Tao *et al*. (1993)
Examined the performance of the CSH algorithm using CRM simulated (consistency check), SSMI and ship borne estimated rainfall and stratiform percentages. Retrieved LH sensitive to surface rainfall amount and stratiform percentage.	Tao *et al.* (2000)
First paper to retrieve LH based on one-month of TRMM-estimated rainfall products.	Tao *et al.* (2001)
Improved CSH by using several CRM-simulations to build the LUTs, individual heating components retrieved separately, LUTs separated into many surface rain rate intensity bins and stratiform fractions	Tao *et al.* (2010)
Improved CSH by using even more CRM simulations with better microphysics at finer resolution to build the LUTs and added new metrics for echo top heights and low-level dBZ gradients to the LUTs	Lang and Tao (2018)
Expanded the retrieval of LH to higher latitudes and the cold season using NU-WRF simulations of synoptic storms to build separate LUTs	Tao *et al*. (2019)
Review papers on LH algorithms, applications and evaluations	Tao *et al.* (2006, 2016)

Table 1 Chronology of the Goddard CSH algorithm with key improvements and references. Adapted from Tao *et al.* (2019)

Input: Combined 2BCMB (DPR + GMI) rainfall products

The CSH algorithm only requires information on surface precipitation rates, amount of stratiform rain, precipitation properties (i.e., radar reflectivity, echo top height, maximum radar reflectivity, freezing level) and the location of the observed cloud systems (i.e., land or ocean, tropics/warm season or higher latitudes/cold season).

Look-Up Tables (LUTs):

The CSH products are based on heating look-up tables (LUTs). The LUTs are produced using two different cloud resolution models: (1) the Goddard Cumulus Ensemble model (GCE) for the tropics (warm season) and (2) the NASA-Unified Weather Research and Forecasting model (NU-

WRF) for higher latitudes (cold season). Please see Figure 1 for a schematic diagram showing the use of the 2BCMB rainfall product to retrieve LH. The figure also shows the required precipitation properties to retrieve LH for the tropics / warm season and higher latitudes / cold season, respectively. Also note that the Level 3 LH product (3GCSH) is a simple area average of the Level 2 product (2HCSH).

(1) CSH algorithm for the tropical region

The LUTs are generated using the GCE at high-resolution to simulate surface rainfall and Q_1 profiles (i.e., LH+Eddy+Qr) that are in very good agreement with sounding estimates.

LUTs derived from multi-week GCE simulations are composited into land and ocean regions. Each set of land/ocean LUTs consists of stored mean latent, radiative and eddy-heating profiles. In addition to the 36 surface rain intensity bins (every 20 mm/day) and convective and stratiform bins, the CSH look-up-tables (LUTs) are further binned according to mean echo top height (5 bins, 0-2, 2-4, 4-6, 6-8, and 8+ km) and low-level (0-2 km AGL) vertical reflectivity gradient (downward increasing or decreasing), which were introduced in V5 (Lang and Tao 2018) to improve heating depth and intensity of low-level evaporative cooling in stratiform regions, respectively. For V6, the CSH LUTs are still composited into land and ocean regions; however, the "near rain" and "far from rain" LUTs for latent heating (LH) are no longer used (i.e., LH is only retrieved for rainy pixels). The CSH land and ocean LUTs are still composited from 6 multi-week ocean cases and 4 multi-week land cases (see Table 2).

Field Campaign	*Geographic Location*	*Dates*	*Modeling Days*	*Reference(s)*
ARM-SGP-97	Land (Southern Great Plains)	June - July, 1997	29	Tao *et al.* (2004); Zeng *et al.* (2009)
ARM-SGP-02		May - June, 2002	20	Zeng *et al.* (2007, 2009)
SCSMEX/NESA	Ocean (South China Sea)	May – June, 1998	45	Tao *et al.* (2003), Zeng *et al.* (2008)
TOGA-COARE	Ocean (Equatorial West Pacific)	November, 1992 – February, 1993	61	Das *et al.* (1999); Johnson *et al.* (2002); Zeng *et al.* (2009)
GATE	Ocean (Tropical Atlantic)	August – September, 1974	20	Tao *et al.* (2004); Zeng *et al.* (2009)
KWAJEX	Ocean (Marshall Islands)	July – September, 1999	52	Zeng *et al.* (2008)
TWP-ICE	Ocean (Darwin, Australian)	January – February, 2006	24	Zeng *et al.* (2013)
MC3E	Land (Southern Great Plains)	April – March, 2011	33	Zeng *et al.* (2007)
DYNAMO	Ocean (Equatorial Indian Ocean)	November – December, 2011	31	Li *et al.* (2018)
GoAMAZON	Land (Amazon Basin)	February – March, 2014	40	Lang and Tao (2018)

Table 2 Field campaigns used to build the current CSH LUTs including their geographic location, starting time and length of integration for the corresponding GCE model simulations. Also listed are GCE modeling papers that have included the case.

(2) **CSH for higher latitudes**

To support GPM, the CSH algorithm needs to include LH profiles associated with higher latitudes (poleward of 35° North/35° South) and the winter season in its LUTs. Large-scale advective forcing derived from sounding networks is unavailable for higher-latitude winter weather events. Therefore, a regional-scale numerical model such as the NASA Unified-Weather Research and Forecasting model (NU-WRF, Peters-Lidard *et al.* 2015) is used as it is better suited to handle precipitation systems associated with high latitude frontal and snow events and cyclones. Six synoptic-scale storm cases are selected for the NU-WRF simulations to generate the cold-season LH LUTs. Three cases are winter storms observed over the eastern continental US (CONUS) in 2014 and 2015. The other three cases are storms that developed over the eastern Pacific off the coast of California during the CalWater 2015 field campaign (Ralph *et al.* 2016).

These results suggest that NU-WRF simulated precipitation quantities can be used to build relationships with LH. Collectively, LH estimates can be made and refined according to the ambient reflectivity/precipitation structures and thus provide the basis by which the CSH algorithm and its LUTs can be expanded to colder environments. Table 3 shows the key parameters, i.e., surface precipitation rate (mm h^{-1}), maximum radar reflectivity height (meters), freezing level height (meters), echo top height (meters), decreasing flag and maximum radar reflectivity intensity (dBZ), which are to be used for the new CSH cold season LH LUT. The bin ranges are based on close examination of the results from the NU-WRF-simulations. Also note that the range of the surface precipitation intensity and other precipitation properties (radar reflectivity, freezing level height) are selected through detailed analysis of the NU-WRF simulations.

Variables	**Bin ranges**
Surface rainfall rate (mm h^{-1})	0., 0.178, 1., 1.78, 3.16, 5.62, 7.5, 10., 13.3, 17.8, 22.4, 27.0, 31.6, 44.0, 56.2, 70.0, 100., 999.
Max dBZ height (m)	0., 500., 1000., 1500., 2000., 3000., 4000., 5000., 99999.
Freezing level height (m)	Negative, 0., 500., 1000., 1500., 2000., 2500., 3000., 3500., 4000., 4500., 5000., 5500, 99999.
Echo top height (m)	0., 1000., 2000., 3000., 4000., 5000., 6000.,7000., 8000., 9000., 10000., 99999.
Decreasing flag	“Decreasing”, “Non-decreasing”
Max dBZ intensity	-10, -8, …78, 80 (from-10 to 80 with an interval of 2)

Table 3 Key parameters used for the CSH cold season LH look-up table. The LUT is built from NU-WRF simulated LH profiles associated with six synoptic storm events. Bin ranges are for V6. Adapted from Tao *et al.* (2019).

Products:

Level 2: Latent heating pixel (2HCSH)
Level 3: Latent heating 0.25 degree gridded orbital (3GCSH)
Level 3: Latent heating 0.25 degree gridded monthly (3HCSH)

Tropical/Warm Season: Each product contains LH, eddy heating, radiative heating, microphysical moistening and eddy moistening.

High Latitudes/Cold Season: Only contains LH.

Figures 2 shows the CSH retrieved 3-month zonal mean vertically-integrated Q_1-Q_R for both TRMM and GPM. The results indicate that the Goddard LH algorithm-retrieved vertically-integrated Q_1-Q_R is quite similar for both TRMM and GPM. Both retrieved "equivalent" surface rain rates are in agreement with the Combined derived, especially over the ITCZ region. Differences occur over the region around 20° – 30° N.

Figure 3 shows the 3-month mean Combined derived surface rain rate and vertically-integrated Q_1-Q_R (equivalent" surface rain rate) at 0.25^o x 0.25^o resolution (level 3 CSH LH product). The results show a very similar pattern (distribution) between the Combined and vertically-integrated Q_1-Q_R equivalent surface rain rate at 0.25^o x 0.25^o resolution. The bottom panel shows the difference between the mean column-integrated 3GCSH cloud diabatic heating and the mean surface rainfall rate from the Combined algorithm. The difference (plot) can be used as a flag for Goddard Latent Heating Retrieval!

Resolution:

Level 2: 5 km horizontal, 80 vertical levels
Level 3: 0.25 degree horizontal, 80 vertical levels

Caveats:

The CSH-derived heating profiles are sensitive to DPR/GMI-derived surface rainfall (affects the magnitude) and stratiform percentage (affects the vertical distribution and level of peak heating).

The CSH latent heating profiles are also sensitive to the LUTs. However, the current LUTs are only based on a limited number of cases (several tropical oceanic but only a few continental; please see Table 2).

References:

Das, S., D. Johnson and W.-K. Tao, 1999: Single-column and cloud ensemble model simulations of TOGA COARE convective systems, *J. Meteor. Soc. Japan*, 77, 803-826.

Johnson, D. E., W.-K. Tao, J. Simpson, and C.-H. Sui, 2002: A study of the response of deep tropical clouds to large-scale thermodynamic forcing. Part I: Modeling strategies and simulations of TOGA COARE convective systems. *J. Atmos. Sci.*, **59**, 3492-3518.

Lang, S. E., and W.-K. Tao, 2018: The next-generation Goddard Convective-Stratiform Heating Algorithm: New tropical and warm season retrievals for GPM. J. Climate, V31, No 5, doi: 10.1175/JCLI-D-17-0224.1.

Li, X., M. Janiga, S. Wang, W.-K. Tao, A. Rowe, W. Xu, C. Liu, T. Matsui, and C. Zhang, 2018: Precipitation structure evolution during November DYNAMO MJO event: Cloud-resolution simulations and comparison with multiple radar observations. *J. Geophys. Res.*, **123**. https://doi.org/10.1002/2017JD027775

Peters-Lidard, C.D., E. M. Kemp, T. Matsui, J. A. Santanello, Jr., S. V., Kumar, J. Jacob, T. Clune, **W.-K. Tao**, M. Chin, A. Hou, J. L. Case,, D. Kim, K.-M. Kim, W. Lau, Y. Liu, J.-J. Shi, D. Starr, Q. Tan,, Z. Tao, B. Zaitchik,

B. Zavodsky, S. Zhang, M. Zupanski, 2014: Integrated Modeling of Aerosol, Cloud, Precipitation and Land Processes at Satellite-Resolved Scales with the NASA Unified-Weather Research and Forecasting Model, *Environmental Modeling & Software* **67**, 149–159. doi: http://dx.doi.org/10.1016/j.envsoft.2015.01.007

Ralph, F.M., K.A. Prather, D. Cayan, J.R. Spackman, P. DeMott, M. Dettinger, C. Fairall, R. Leung, D. Rosenfeld, S. Rutledge, D. Waliser, A.B. White, J. Cordeira, A. Martin, J. Helly, and J. Intrieri, 2016: CalWater Field Studies Designed to Quantify the Roles of Atmospheric Rivers and Aerosols in Modulating U.S. West Coast Precipitation in a Changing Climate. Bull. Amer. Meteor. Soc., 97, 1209–1228, https://doi.org/10.1175/BAMS-D-14-00043.1

Tao, W.-K., J. Simpson, S. Lang, M. McCumber, R. Adler, and R. Penc, 1990: An algorithm to estimate the heating budget from vertical hydrometeor profiles. J. Appl. Meteor., 29, 1232-1244.

Tao, W.-K., S. Lang, J. Simpson, and R. Adler, 1993: Retrieval algorithms for estimating the vertical profiles of latent heat release: Their applications for TRMM. J. Meteor. Soc. Japan, 71, 685-700.

Tao, W.-K., S. Lang, J. Simpson, W.S. Olson, D. Johnson, B. Ferrier, C. Kummerow, and R. Adler, 2000: Retrieving vertical profiles of latent heat release in TOGA COARE convective systems using a cloud resolving model, SSM/I and radar data. J. Meteor. Soc. Japan, 78, 333-355.

Tao, W.-K., S. Lang, W.S. Olson, S. Yang, R. Meneghini, J. Simpson, C. Kummerow, E. Smith and J. Halverson, 2001: Retrieved vertical profiles of latent heating release using TRMM rainfall products for February 1998. J. Appl. Meteor., 40, 957-982.

Tao, W.-K., E.A. Smith, R.F. Adler, Z.S. Haddad, A.Y. Hou, T. Iguchi, R. Kakar, T.N. Krishnamurti, C.D. Kummerow, S. Lang, R. Meneghini, K. Nakamura, T. Nakazawa, K. Okamoto, W.S. Olson, S. Satoh, S. Shige, J. Simpson, Y. Takayabu, G.J. Tripoli, and S. Yang, 2006: Retrieval of latent heating from TRMM measurements. Bull. Amer. Meteor. Soc., 87, 1555-1572.

Tao, W.-K., C.-L. Shie, R. Johnson, S. Braun, J. Simpson, and P.E. Ciesielski, 2003: Convective systems over the South China Sea: Cloud resolving model simulations. *J. Atmos. Sci.*, **60**, 2929-2956.

Tao, W.-K., D. Johnson, C.-L. Shie, and J. Simpson. 2004: Atmospheric energy budget and large-scale precipitation efficiency of convective systems during TOGA COARE, GATE, SCSMEX and ARM: Cloud-resolving model simulations, *J. Atmos. Sci*., **61**, 2405-2423.

Tao, W.-K., S. Lang, X. Zeng, S. Shige, and Y. Takayabu, 2010: Relating convective and stratiform rain to latent heating, *J. Climate*, **23**, 1874-1893.

Tao, W.-K., Y. N. Takayabu, S. Lang, S. Shige, W. Olson, A. Hou, X. Jiang, C. Zhang, W. Lau, T. Krishnamurti, D. Waliser, M. Grecu, P. Ciesielski, R. Johnson, R. Houze, R. Kakar, N. Nakamura, S. Braun, S. Hagos, R. Oki, and A. Bhardwaj, 2016: TRMM latent heating retrieval: Applications and comparisons with field campaigns and large-scale analyses, *AMS Meteorological Monographs - Multi-scale Convection-Coupled Systems in the Tropics. Chapter 2*, doi:10.1175/AMSMONOGRAPHS-D-15-0013.1

Tao, W.-K., T. Iguchi, and S. Lang, 2019: Expending the Goddard CSH Algorithm for GPM: New Extra-tropical Retrievals. *J. Applied Meteor. Climatol*., **58**, 921-946, doi: 10.1175/JAMC-D-18-0215.1

Zeng, X., W.-K. Tao, M. Zhang, S. Lang, C. Peters-Lidard, J. Simpson, S. Xie, S. Kumar, J. V. Geiger, C.-L. Shie, and J. L.. Eastman, 2007: Evaluation of long-term cloud-resolving modeling with observational cloud data. *J. Atmos. Sci.*, **64**, 4153-4177.

Zeng, X., W.-K. Tao, S. Lang, A. Hou, M. Zhang, and J. Simpson, 2008: On the sensitivity of Atmospheric ensemble to cloud microphysics in long-term cloud-resolving model simulations. *J. Meteor. Soc. Japan***,** *Special Issue on high-resolution cloud models***, 86A**, 45-65.

Zeng, X., W.-K. Tao, M. Zhang, A. Y. Hou, S. Xie, S. Lang, X. Li, D. Starr, and X. Li, 2009: A contribution by ice nuclei to global warming. *Q. J. R. Met. Soc*., **135**, 1614-1629, DOI: 10.1002/qj.449.

Zeng, X., W.-K. Tao, S. Powell, R. Houze, Jr., P. Ciesielski, N. Guy, H. Pierce and T. Matsui, 2013: Comparison of Water Budget between AMMA and TWP-ICE Clouds. *J. Atmos. Sci.*, **70**, 487-503. doi.org/10.1175/JAS-D-12-050.1

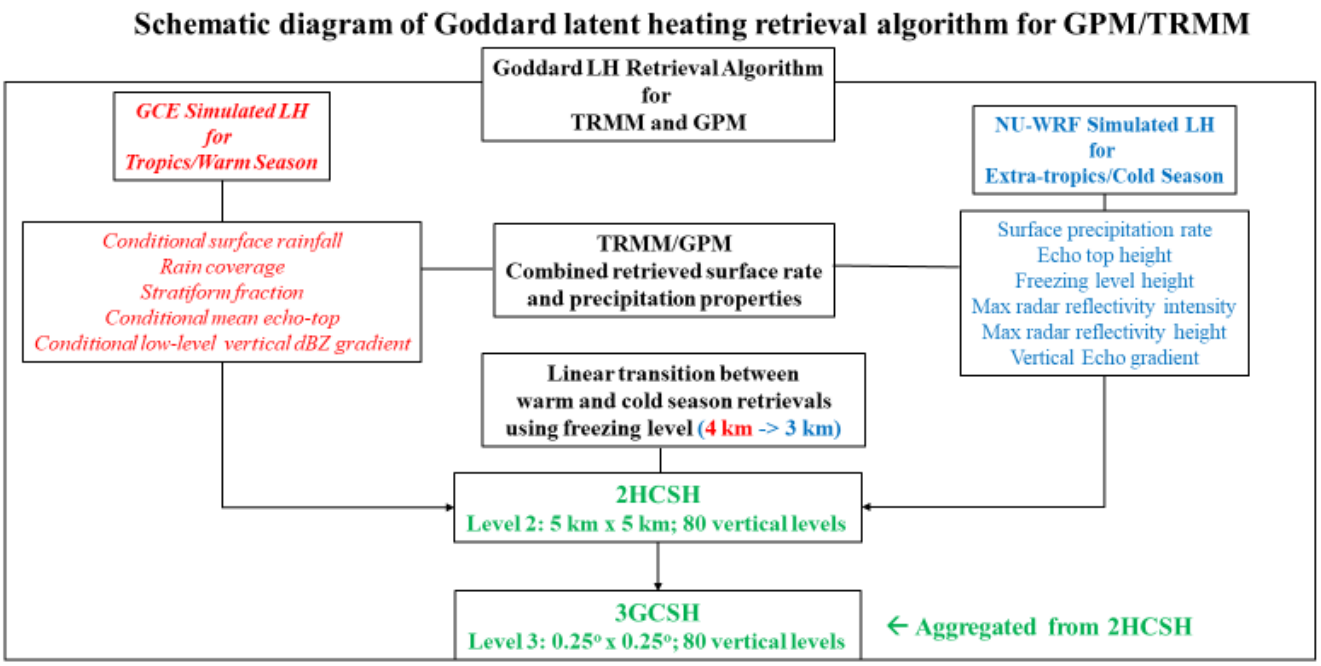

Figure 1 Schematic diagram using 2BCMB rainfall product to retrieve LH for GPM AND TRMM.

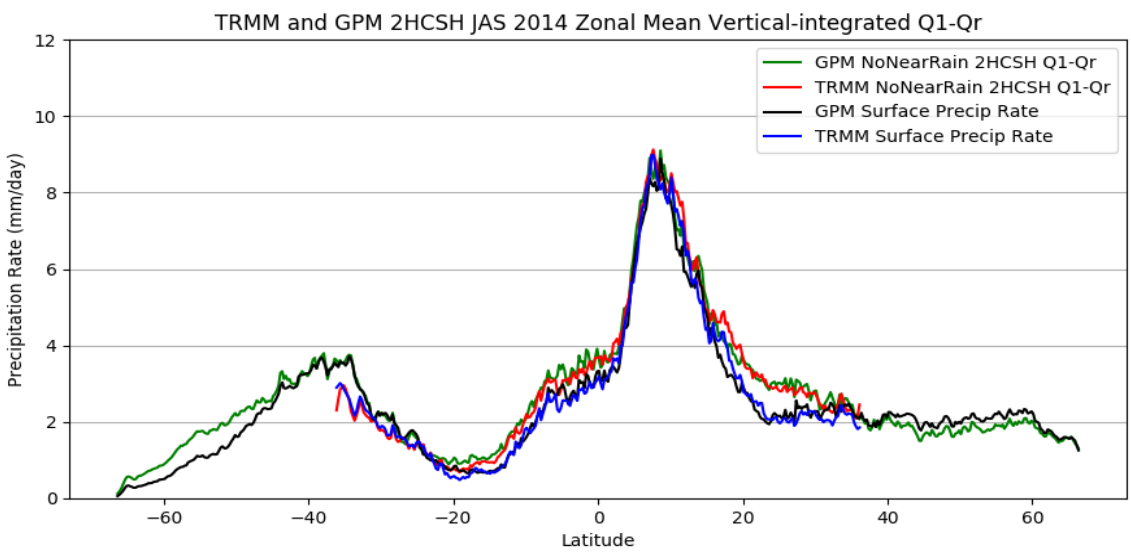

Figure 2 2HCSH retrieved 3-month zonal mean vertically-integrated Q_1-Q_R for TRMM and GPM.

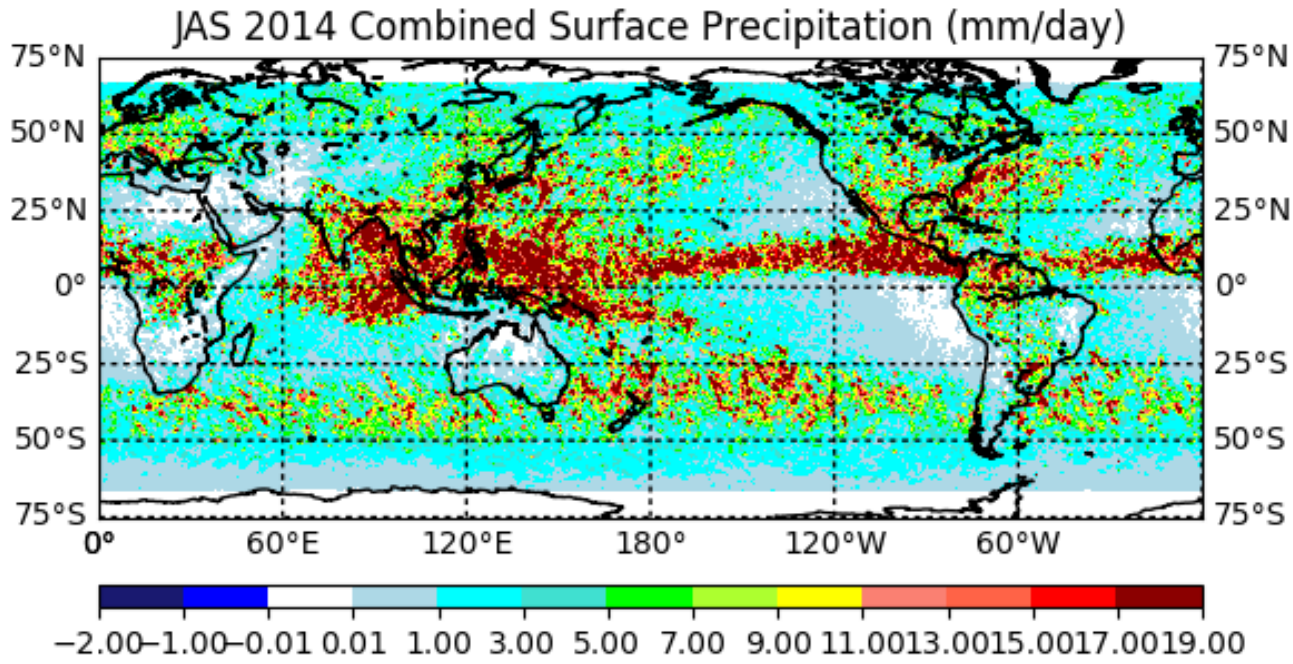
JAS 2014 Combined Surface Precipitation (mm/day)
75°N
50°N
25°N
0°
25°S
50°S
75°S
0°
60°E
120°E
180°
120°W
60°W
−2.00 −1.00 −0.01 0.01 1.00 3.00 5.00 7.00 9.00 11.00 13.00 15.00 17.00 19.00

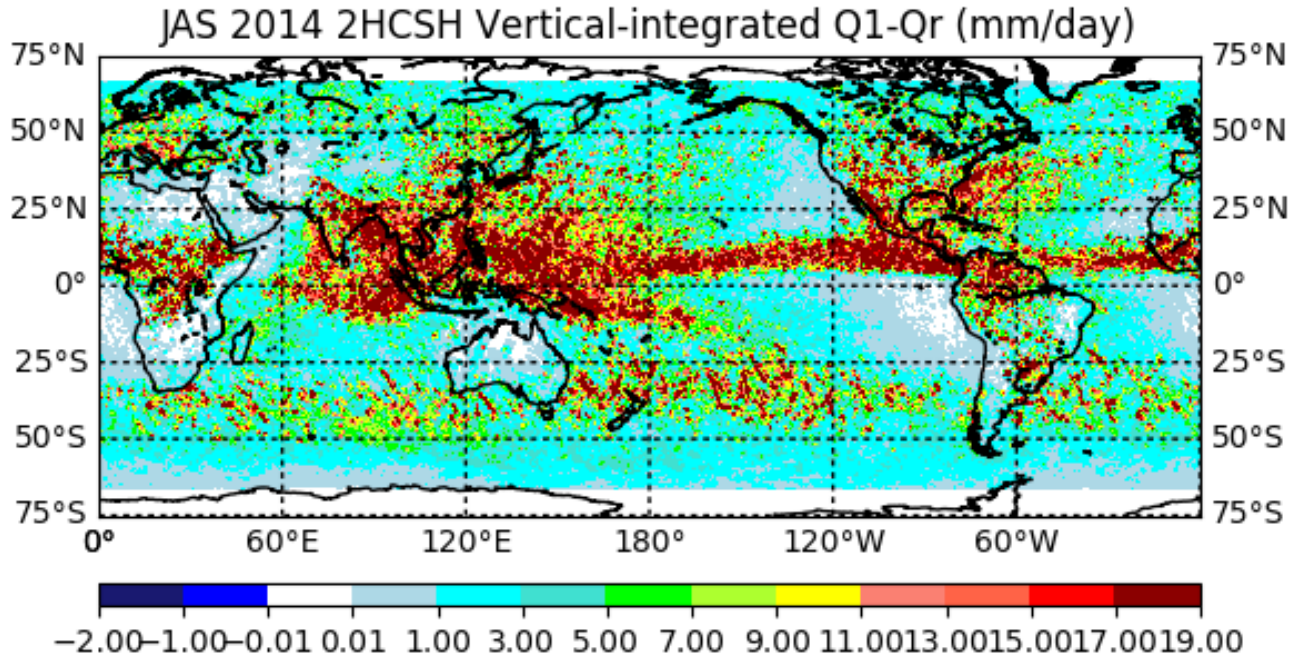
JAS 2014 2HCSH Vertical-integrated Q1-Qr (mm/day)
75°N
50°N
25°N
0°
25°S
50°S
75°S
0°
60°E
120°E
180°
120°W
60°W
−2.00 −1.00 −0.01 0.01 1.00 3.00 5.00 7.00 9.00 11.00 13.00 15.00 17.00 19.00

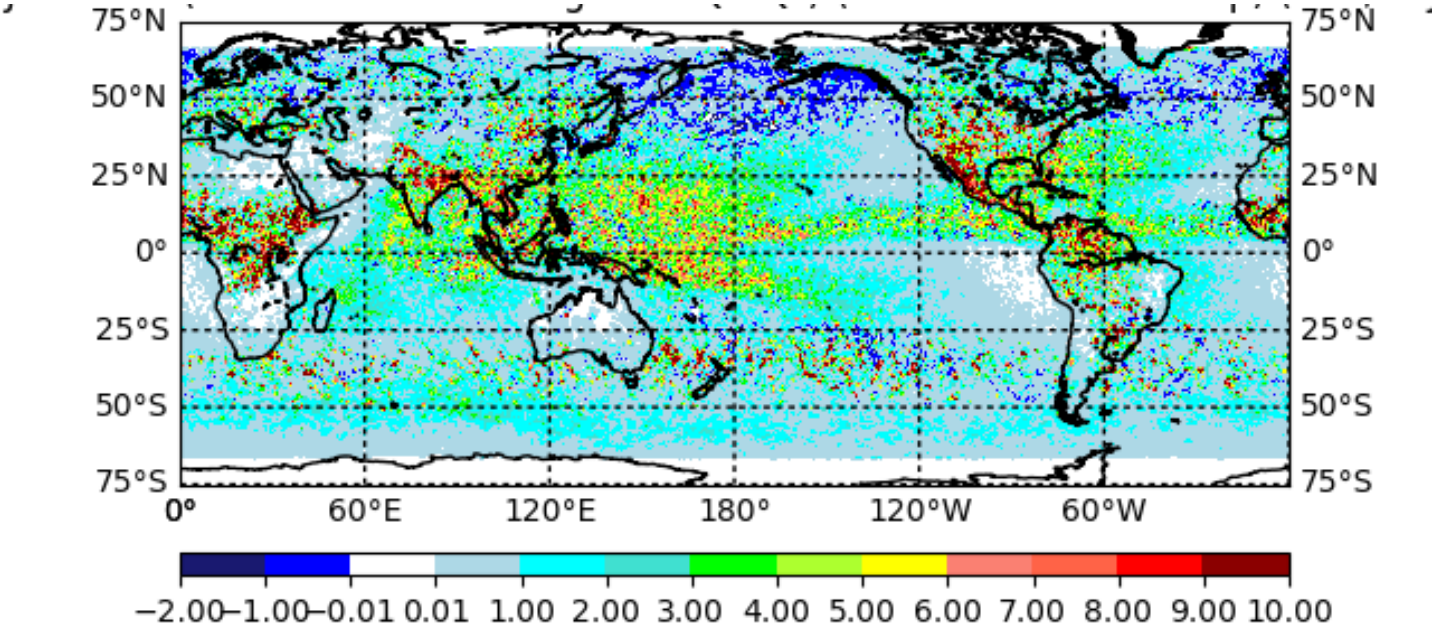

Figure 3 Three-month mean Combined derived surface rain (top panel) and CSH vertically-integrated Q_1-Q_R (equivalent" surface rain rate) (middle panel) at 0.25° x 0.25° resolution. The bottom panel is the difference between the CSH equivalent and Combined surface rain.